ARTICLE NO. 79-4130

Prediction of Critical Mach Number for Store Configurations

James W. Purvis* and John E. Burkhalter†
Auburn University, Auburn, Ala.

A numerical method is described and applied to the prediction of the critical Mach number of store configurations. A finite volume integral method is used to solve the full nonlinear potential equation in conservation of mass form. With the density held constant, the entire potential flowfield is solved by matrix iteration. The density field is then relaxed using the new potential values. The use of central differences for the velocity everywhere in the field is made possible by special treatment of the density terms in the coefficient matrix. The finite volume concept allows the boundary conditions to be treated in a simple and exact manner, without the use of a mapping scheme. Results are obtained for configurations that range from very thin pointed bodies to hemispherically blunt bodies. Excellent agreement is obtained for the pressure distribution over each body, even in supercritical flows, and the critical Mach number is easily and accurately computed. Finally, the computational advantages and capabilities of the numerical method are discussed and compared with other existing codes.

Nomenclature

a = speed of sound, cm/s
a_{nm} = matrix (index notation and rules used throughout)
b_m = vector
C_p = pressure coefficient, $2(p-p_\infty)/\rho_\infty V_\infty^2$
I_{nm} = identity matrix
I_ρ = integer function of density ratio, Eq. (27)
M = Mach number
T' = absolute temperature, K
u,v = nondimensional velocity components (ϕ_x,ϕ_r)
V = velocity, cm/s
ω = relaxation parameter
x,r = polar coordinates
γ = specific heat ratio
∇ = gradient operator
ϕ = nondimensional total potential function
ρ = nondimensional density, ρ'/ρ'_∞
ρ' = fluid density, gm/cm^3

Subscripts

$(\ )_x$ = partial derivative with respect to x
$(\ )_\infty$ = freestream condition

Introduction

ANALYTICAL methods for the efficient prediction of critical Mach number flowfields for store configurations have a variety of uses in current aerodynamic research and design problems. The effects of nonlinear terms in the conservation equations, which become very significant at speeds approaching the critical Mach number, are of particular interest. An accurate analysis that includes the nonlinear terms can provide upper limits on the range of validity of linear theory methods, such as those used in the prediction of the interference load distribution for external stores mounted on a triple ejector rack.[1,2] Another use of accurate critical Mach number flowfields is to provide more precise inputs on wave drag and drag rise Mach number for engineering design tools such as the aeroprediction code of Ref. 3.

The present work presents a numerical method that is used to efficiently solve for the steady isentropic flow about axisymmetric store configurations in critical Mach number flows. Viscous terms in the conservation equations are neglected based on Prandtl's hypothesis.[4] Under the above assumptions, the conservation and state variable equations reduce to a single form—the nonlinear potential equation.

Although some limited analytical methods exist,[5,6] the significant nonlinear terms indicate a numerical approach. Examples of the major numerical methods applicable to such problems include finite difference schemes (both relaxation[7] and time-dependent approaches to steady state[8-9]), the finite element method,[10-12] the method of integral relations,[13,14] and the relatively new method of projections.[15-18] Most of these methods may be eliminated from consideration due to either excessive computer execution time, excessive storage requirements, or complexity of coding. Relaxation methods, however, have been used with great success following the initial effort by Murman and Cole[7] for solving subsonic flows with embedded supersonic regions. In particular, a notable work is that of South and Jameson[19] for axisymmetric bodies. Unfortunately, a detailed examination of their results shows that values of minimum pressure are significantly in error, even though overall results are quite good. Accurate calculation of minimum pressure is necessary to determine the onset of wave drag.

Recently, numerical methods for solving transonic flows have been proposed with the objectives of increased accuracy, better representation of the body boundary conditions, and improved convergence, i.e., shorter computation times.[20-24] Increased accuracy and computational efficiency has been obtained by solving a finite volume integral equation[21-23] expressed in surface flux form, rather than the familiar differential forms of the governing equation(s). However, the schemes all involve time-dependent (or pseudo-time-dependent) relaxation of the dependent variable(s). The major difficulty in numerical works, that of sufficiently accurate discrete approximations to the body boundary conditions, is usually handled with body fitted coordinates and complex mapping schemes. Accelerated convergence may be obtained by approximate factorization schemes[20] that lead to Poisson equations. In such semidirect methods, the entire flowfield is solved at once during an iteration sequence with a direct elliptic solver. These methods usually exhibit faster convergence than methods such as point or line relaxation[24] when the freestream is subsonic, because changes are felt simultaneously at all points in the field during each iteration.

Received Sept. 25, 1978; revision received April 9, 1979. Copyright © American Institute of Aeronautics and Astronautics, Inc., 1979. All rights reserved. Reprints of this article may be ordered from AIAA Special Publications, 1290 Avenue of the Americas, New York, N.Y. 10019. Order by Article No. at top of page. Member price $2.00 each, nonmember, $3.00 each. **Remittance must accompany order.**

Index categories: Computational Methods; Subsonic Flow; Transonic Flow.

*Presently, Aerospace Engineer, Naval Surface Weapons Center; formerly, Assistant Professor, Aerospace Engineering. Member AIAA

†Assistant Professor, Aerospace Engineering. Member AIAA.

The present work combines many of the above ideas in a relaxation method for predicting pressure distributions and the critical Mach number of axisymmetric store configurations. The full potential equation is recast into a special conservation form for an iterative solution that is shown to be the nondimensional continuity equation. Integration of the continuity equation over a finite volume and use of the divergence theorem allow replacement of the volume integral with a surface integral, which is then put in finite difference form. This form is not used in any of the usual finite difference approaches, and has the advantage that only first-order derivatives appear while derivatives of the iteration variable are not present.

The present formulation leads to a large system of equations that must be solved simultaneously; however, the solution technique does not require storage or inversion of a large coefficient matrix. Upwind difference equations involving the velocity are not required, and the system of equations to be solved during each iteration does not contain any nonlinear equations. The method of solution allows disturbances in elliptic regions to propagate throughout the field in each successive iteration. A double relaxation is performed during each iteration, first solving a linear set of equations for the potential using an iterative matrix solver, then relaxing the nondimensional density for rapid convergence. The physical flow requirement of no upstream disturbance propagation in supersonic zones is uniquely satisfied through the use of central or backward Taylor series expansions for the density.

Using a concept from the finite element method, body surface boundary conditions, which are usually a major problem in finite difference methods,[19, 25-28] are shown to be simple and exact even for blunt-nosed bodies. Further, the inverse radius term $1/r$, which usually appears in axisymmetric problems, does not occur in the present formulation and hence does not lead to difficulties near the radial axis. In general, the present method does not require any special formulas or techniques for the treatment of boundary conditions and iterative stability. The accuracy of the numerical results is verified by comparison with experimental data for several typical store configurations.

General Theory

Conservation and State Variable Equations

The governing equations for fluid flow can be written by considering the conservation of mass (continuity), conservation of momentum, conservation of energy and an equation of state. Under the assumptions of steady, isentropic, inviscid flow, these equations are reduced to a single differential equation. The restriction of irrotationality, imposed by the previous assumptions, allows the introduction of the velocity potential. The governing equation may then be expressed in nondimensional form as:

$$\nabla \cdot (\rho \nabla \phi) = 0 \tag{1}$$

where ϕ is the nondimensionalized total velocity potential. Since the flow is isentropic, the nondimensional density ρ may be expressed uniquely in terms of the velocity potential:

$$\rho \left[1 + \tfrac{1}{2}(\gamma - 1) M_\infty^2 (1 - \nabla\phi \cdot \nabla\phi) \right]^{1/(\gamma-1)} \tag{2}$$

Equation (1), when expanded using Eq. (2) and expressed in terms of the perturbation potential, is the familiar "full potential equation."[4]

To formulate the problem for the computer solution, the divergence theorem is applied to the integral form of the governing Eq. (1) resulting in

$$\int\int\int_V \nabla \cdot (\rho \nabla \phi) \, dV = \int\int_S \rho \nabla \phi \cdot \bar{n} \, dS = 0 \tag{3}$$

where S is the boundary surface enclosing the volume and $\bar{n}$ is the unit outward normal on the surface S. With a sign change, Eq. (3) becomes:

$$-\int\int_V \rho \nabla \phi \cdot \bar{n} \, dS = 0 \tag{4}$$

Equation (4) is solved numerically as discussed in the following sections.

Computational Grid Formulation

The domain in which Eq. (4) is to be solved is subdivided with a rectangular mesh or grid, and initial values of ρ are assumed at the center (denoted by ● 's in Fig. 1) of each "cell" in the grid. Equation (4) is applied to each cell in the grid and evaluated in terms of the potential at the center of each cell.

For axisymmetric flows, Eq. (4), as applied to cell (i,j) shown in Fig. 1, is:

$$\rho_1 u_1 s_1 + \rho_2 v_2 s_2 - \rho_3 u_3 s_3 - \rho_4 v_4 s_4 = 0 \tag{5}$$

To obtain Eq. (5), the integral in Eq. (4) was evaluated assuming a linear distribution of ρu or ρv along each surface s, which is equivalent to assuming a second order distribution of ϕ along each cell surface in a finite element method. The values in Eq. (5) are then the values at the center of each surface, or, equivalently, the average of ρu or ρv along s.

Referring to Fig. 1, the areas for three-dimensional axisymmetric flow are

$$s_1 = \pi r_{e_{j+1}}^2 - \pi r_{e_j}^2 \tag{6}$$

$$s_2 = 2\pi r_{e_j} (x_{e_{i+1}} - x_{e_i}) \tag{7}$$

where r_e represents the radial coordinate.

The values of density and velocity in Eq. (5) may be expressed in terms of values at the center of the cells with the aid of Taylor series expansions.

For the density, truncating the higher order terms in a central expansion about point 1 gives:

$$\rho_1 = \tfrac{1}{2}(\rho_{i,j} + \rho_{i-1,j}) \tag{8}$$

The nondimensional velocity components are all first partial derivatives of the potential. Expanding about the center of the cell wall and truncating higher order terms results in the well known central difference formula:

$$u_1 = (\phi_{i,j} - \phi_{i-1,j}) / \Delta x \tag{9}$$

Equations (8) and (9) are both second-order accurate with respect to half of the mesh spacing Δx.

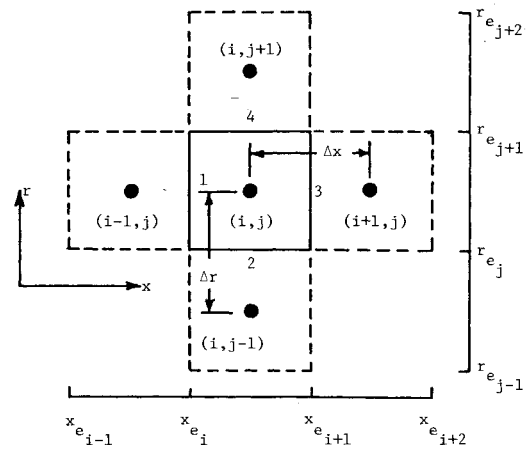

Fig. 1 Computational cell.

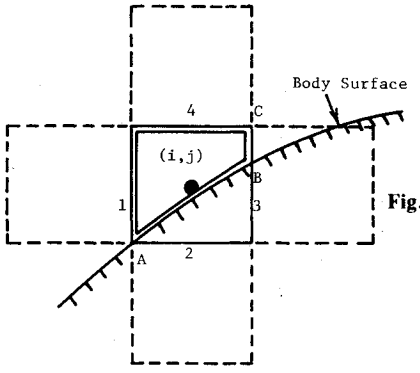

Fig. 2 Body boundary cell.

Body Boundary Conditions

One of the most difficult aspects of finite difference methods to date has been the treatment of body boundary conditions. The opposite is true in the finite element method, since the sides of certain elements approximate the body surface. Finite volume methods combine the simplicity of calculations of the finite difference method with the relatively simple finite element treatment of body boundary conditions. The present formulation applies the finite volume ideas; however, special nonorthogonal body-fitted cells are not required.

Consider the cell cut by the body surface as shown in Fig. 2. The surface integral for this cell is taken around the boundary shown by the double solid line. Since the body boundary condition of no flow normal to the surface, $\bar{V}\cdot\bar{n}=0$, requires that there be no flow through surface AB, then the equivalent expression, Eq. (5), is:

$$\rho_1 u_1 s_1 - \rho_3 u_3 s_3 - \rho_4 v_4 s_4 = 0 \tag{10}$$

where s_3 is now the area of segment BC. Note that this equation is exact for any size cell, and that no interpolation, contour mapping, or other scheme is required.

Numerical Procedure

Using Eqs. (6-9), Eq. (5) for cell (i,j) can be arranged into:

$$C_1\phi_{i-1,j} + C_2\phi_{i,j-1} + C_3\phi_{i+1,j} + C_4\phi_{i,j+1} + C_5\phi_{i,j} = 0 \tag{11}$$

where the constants C_n are, for example:

$$C_1 = -(\rho_{i,j} + \rho_{i-1,j})s_1/2\Delta x \tag{12}$$

and

$$C_5 = -(C_1 + C_2 + C_3 + C_4) \tag{13}$$

Ordering the discrete grid values of the potential into a vector, the system of Eq. (11) for each cell leads to the matrix formulation:

$$a_{nm}\phi_m = b_n \,, m = 1,2,\ldots,M = i_{\max}\cdot j_{\max} \tag{14}$$

with:

$$n = i + i_{\max}\cdot(j-1) \tag{15}$$

The coefficient matrix a_{nm} consists of the constants C_1-C_5 on each row with all other elements zero. The forcing vector b_n is zero for all interior and body surface cells. For the far-field boundary cells, the entries in b_n are determined from the appropriate cell areas and either uniform flow conditions or slender body theory values.

The matrix in Eq. (14) is large, banded, and very sparse, which makes it desirable to use an iterative method to solve

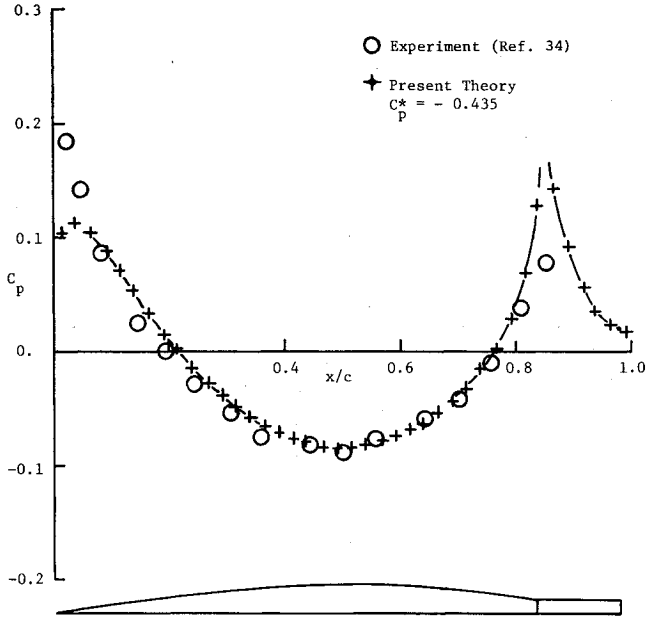

Fig. 3 Variation of pressure coefficient for parabolic body, $M_\infty = 0.80$.

the system. The system is first rewritten as

$$\phi_n = \hat{a}_{nm}\phi_m + B_n \tag{16}$$

where

$$\hat{a}_{nm} = I_{nm} - a_{nm}/a_{nn} \tag{17}$$

and

$$B_n = b_n/a_{nn} \tag{18}$$

Convergence of an iterative method such as accelerated Gauss-Siedel is then guaranteed if some norm of $\hat{a}_{nm}$ is less than unity.[29] By virtue of its construction

$$0 \le \hat{a}_{nm} < 1 \tag{19}$$

and

$$\sum_m \hat{a}_{nm} \le 1 \tag{20}$$

Then clearly the norm

$$\|\hat{a}_{nm}\| = \max_n \sqrt{\sum_m \hat{a}_{nm}^2} \tag{21}$$

is less than unity and an iterative method based on Eq. (16) will always converge.

Since there are at most only four nonzero entries in any row of $\hat{a}_{nm}$, the entire matrix and the vector B_n may be stored in only four column vectors. The kth iteration of the Gauss-Siedel solution algorithm based on Eq. (16) is then:

$$\phi_n^{k+1/2} = A_{1_n}\phi_{n-1}^{k+1/2} + A_{2_n}\phi_{n-i\max}^{k+1/2} + A_{3_n}\phi_{n+1}^{k} + A_{4_n}\phi_{n+i\max}^{k} + B_n \tag{22}$$

where, for example:

$$A_{1_n} = -(C_1/C_5)_{n\text{th cell}} \tag{23}$$

Note that Eq. (22) is exact in the limit of vanishing cell size, that only first derivatives of the dependent variable were

required, and that the equations for ρ, u, and v used to develop Eq. (22) are second-order accurate.

For a given density field, Eq. (22) is solved iteratively and over-relaxed, using new values for ϕ as they become available. For example, on the kth iteration:

$$\phi_n^{k+1} = \omega\phi_n^{k+1/2} + (1-\omega)\phi_n^k \tag{24}$$

where $\omega = 1.75$ (Ref. 18) for optimum convergence rate. Once each value of ϕ in the field has converged to within a specified tolerance, the matrix iteration is halted. The tolerance depends on both machine accuracy and relative convergence of the density field. New values for density are calculated using the current grid solution for ϕ and Eq. (2). A new coefficient matrix is formulated, and the entire procedure repeated until all values of density in the grid converge to within a desired tolerance for several successive cycles.

To solve Eq. (2), the potential gradient (nondimensional velocity components) must be evaluated at the center of each cell. A multitude of difference equations, central, upwind, and combinations of the two, may be created by appropriate combinations of forward and backward Taylor series expansions. The use of upwind differencing in supersonic regions is well established in the literature and both first- and second-order-accurate forms have been used. Murman and Cole[7] introduced mixed difference operators in the evaluation of the potential gradient, which led to a system of nonlinear simultaneous equations for the potential. South and Jameson[19] found that only the central difference expression was needed for the velocity as long as the appropriate central or upwind operator was used for the velocity gradient. In the present method, the central difference expression

$$u_{i,j} = (\phi_{i+1,j} - \phi_{i-1,j})/2\Delta x \tag{25}$$

is used in both subsonic and supersonic zones, thus eliminating the need for testing and switching to an appropriate operator. As with Eq. (9) for u at the cell sides, Eq. (25) is second-order accurate. There is a physical flow requirement in supersonic zones that disturbances must not be allowed to propagate upstream. In the present method this requirement is met by using two different interpolation schemes for evaluation of the density at the cell sides. Both interpolations are combined in a single expression (see Fig. 1 for notation):

$$\rho_1 = \rho_{i-1,j} + \tfrac{1}{2}[I_\rho(\rho_{i,j} - \rho_{i-1,j}) + (1-I_\rho)(\rho_{i-1,j} - \rho_{i-2,j})] \tag{26}$$

where the integer function I_ρ is

$$I_\rho = \text{Integer}\ (\rho_0/\rho_s) \tag{27}$$

ρ_0 is the linear interpolate

$$\rho_0 = \tfrac{1}{2}(\rho_{i,j} + \rho_{i-1,j}) \tag{28}$$

and ρ_s is the nondimensional density at local sonic velocity

$$\rho_s = \left[1.2\Big/\left(1 + \frac{\gamma-1}{2}M_\infty^2\right)\right]^{1/(\gamma-1)} \tag{29}$$

I_ρ is always zero or unity, depending on whether ρ_0 is greater or less than the sonic value. For subsonic points, Eq. (26) reduces to the previous Eq. (8). At supersonic points, Eq. (26) is a second-order-accurate interpolation based only on upstream values. Thus, changes in the density in the downstream cell cannot influence the density at point 1 if point 1 is locally supersonic. Although Eq. (26) reduces to Eq. (8) if point 1 is exactly sonic, the probability of this situation occurring is low in lieu of computer roundoff errors.

With any numerical method, the closer the initial guess is to the answer, the faster the convergence. In the present method, a simplified form of slender-body theory, using superimposed solutions from the linearized potential equation, is employed to generate initial values of ϕ and ρ in the grid. Each centerline segment of the body lying in the cell is assumed to be a source filament of constant strength. The strength is proportional to the value of the body surface slope as evaluated at the midpoint of the segment. The initial value of ϕ at any point is then the sum of the contribution from each segment.[31]

Results

The primary objective of this work was the development of an accurate, computationally efficient method for predicting the critical Mach number of general store configurations. To assess the accuracy of the method, comparisons of numerical results with experiment are presented in Figs. 3-9 for several axisymmetric bodies. The figures have experimental and theoretical values of nondimensional pressure coefficient C_p plotted versus nondimensional body lengths. The critical pressure coefficient C_p^* is listed on the figure and shown on the axis where appropriate. The body shape is shown schematically below each figure. Finally, calculated minimum pressure coefficients are plotted versus freestream Mach number to determine the critical Mach number of a representative store configuration.

Subcritical Results

Results for a slender three-dimensional body at a freestream Mach number of 0.8 are shown in Fig. 3. The body is a fineness ratio 10 parabolic body of revolution with a constant diameter sting beginning at about 85% of the body length. The body is contained in a region 40 cells long and approximately 1 cell high. The numerical results deviate from experiment at the nose and at the sting-body juncture. These errors were expected for this problem, since no attempt was made to fair the body smoothly into the sting (as the boundary layer would in reality) and the potential flow at the sharp, pointed nose will not exhibit the same characteristics as the real viscous flow. The cell coarseness does not model the nose region well. However, in all other regions of the body the present theory agreed remarkably well with experimental data.

Figures 4 and 5 present data for an M117 store at freestream Mach numbers of 0.5 and 0.8. The M117 is a fairly blunt axisymmetric body consisting of a tangent-ogive nose section, a cylindrical midsection, and a straight-tapered boattail. The body length is nondimensionalized with respect to the body diameter d. In Fig. 4, the body is modeled with a length of 48 cells, and in Fig. 5, the body is 40 cells long; in both cases, the body is 5 cells high. The effect of sting location on the pressure distribution is illustrated comparatively in the two figures. The theoretical sting, shown in the schematic below each plot, begins at different locations for the two cases: 4.8 body diameters aft of the nose in Fig. 4 and 4.0 body diameters aft in Fig. 5. The predicted and measured pressure distributions indicate that the sting probably begins at about 4.3 diameters. The agreement between theory and experiment is excellent in both cases, even at the higher Mach number, and particularly over the nose of the body. The agreement near the sting would have been better had the proper sting location been used, with the body faired into the sting to simulate the boundary layer effect as in Ref. 19.

Figure 6 represents data for three-dimensional axisymmetric flow over a "maximum volume" store at a freestream Mach number of 0.5. The store consists of a hemispherical nose, a straight cylindrical midsection, and a tangent ogive faired into a straight tapered boattail. This configuration is a severe test of the theory, due to the nose bluntness and curvature. Overall agreement between theory and experiment is excellent for this case, particularly on the nose. The slight

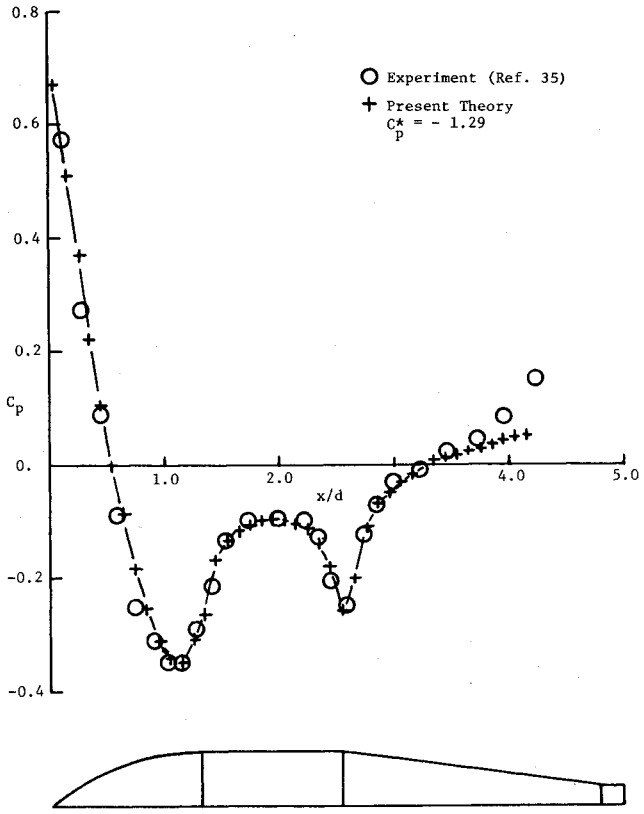

Fig. 4 Variation of pressure coefficient for M117 store, $M_\infty = 0.5$.

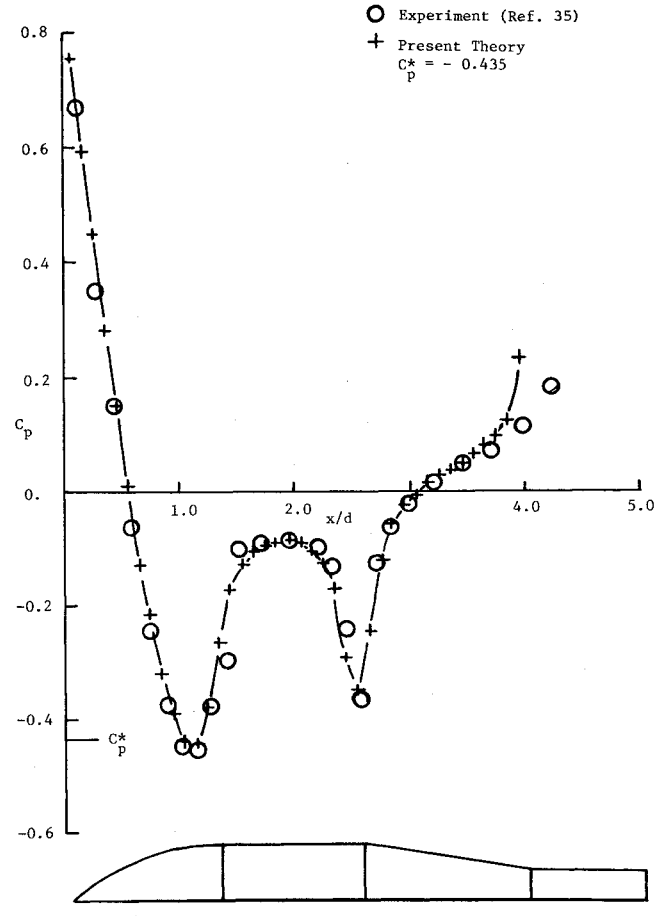

Fig. 5 Variation of pressure coefficient for M117 store, $M_\infty = 0.8$.

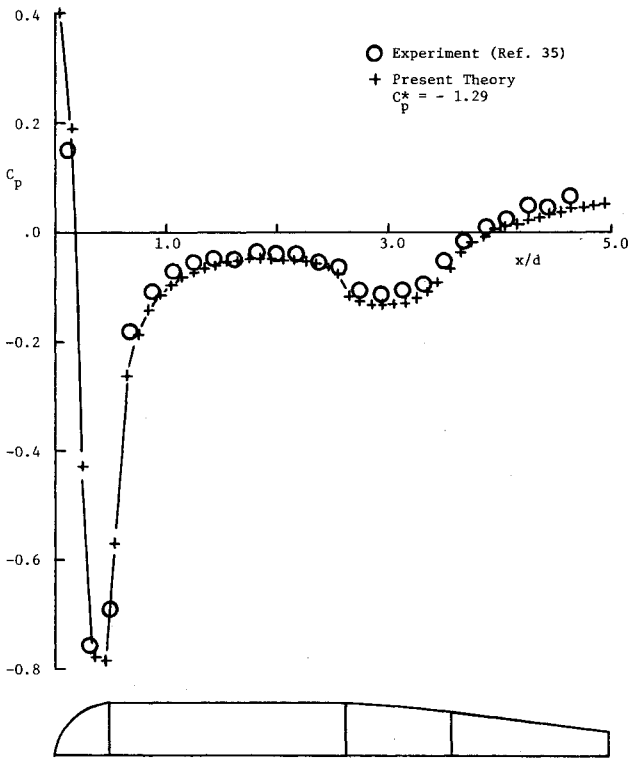

Fig. 6 Variation of pressure coefficient for hemispherical nose store, $M_\infty = 0.5$.

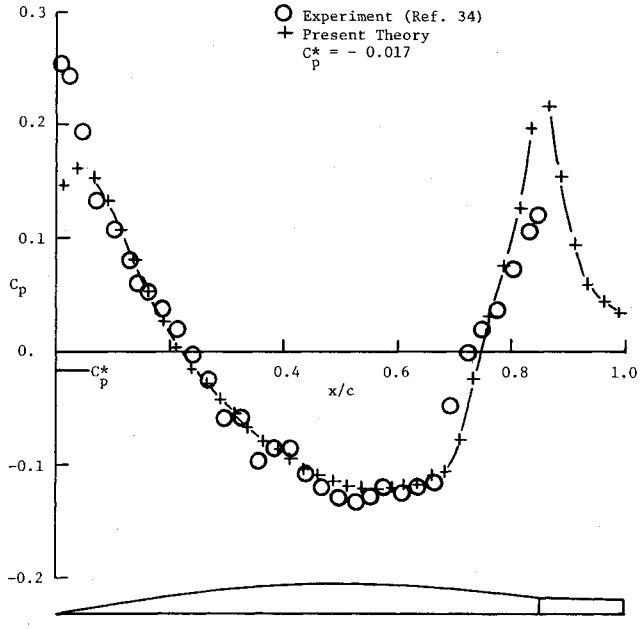

Fig. 7 Variation of pressure coefficient for parabolic body, $M_\infty = 0.99$.

differences on the aft section of the body have been attributed to possible tunnel flow angularities. This particular configuration best illustrates the versatility and accuracy of the method.

Transonic Results

Although the numerical method was devised primarily for application in the subcritical flow regime, the ability to predict transonic effects is necessary since an analyst would not know beforehand when an embedded supersonic zone and possibly a shock might appear. In order to illustrate the capability of the method in supercritical flows, calculations

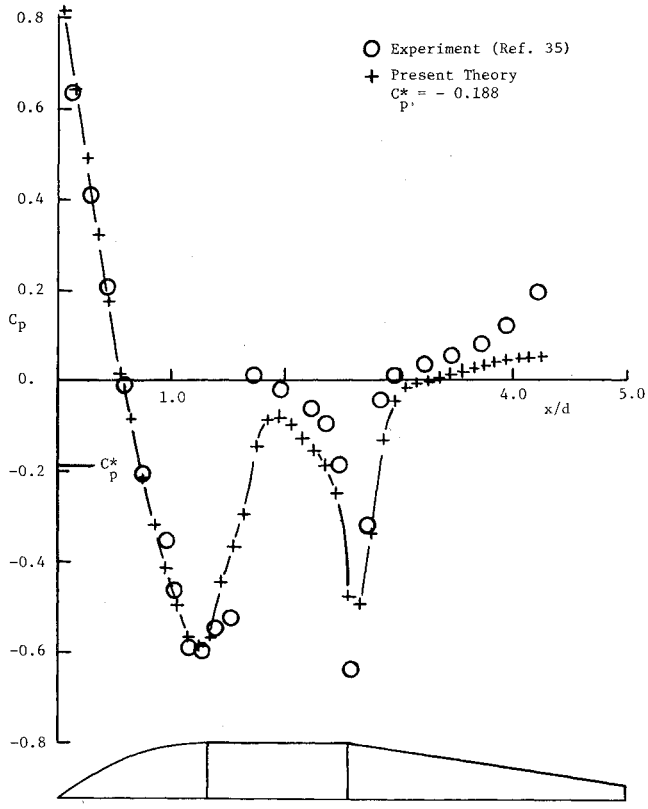

Fig. 8 Variation of pressure coefficient for M117 standard store, $M_\infty = 0.9$.

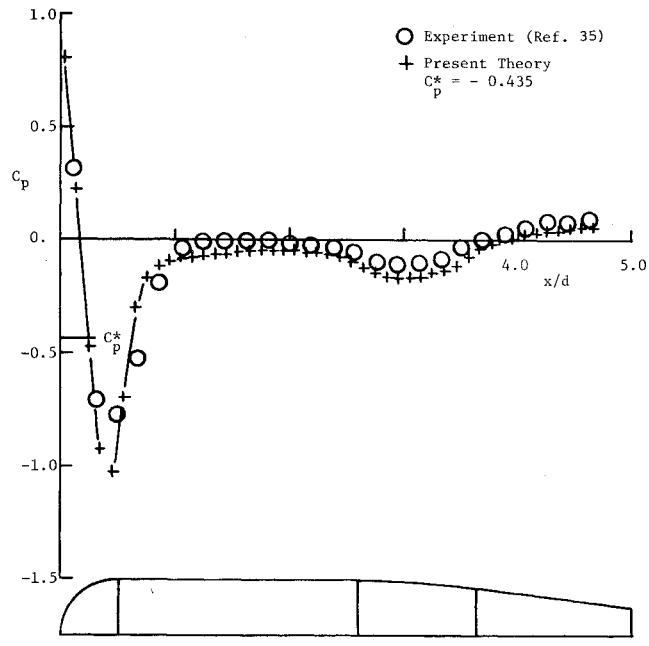

Fig. 9 Variation of pressure coefficient for hemispherical nose store, $M_\infty = 0.8$.

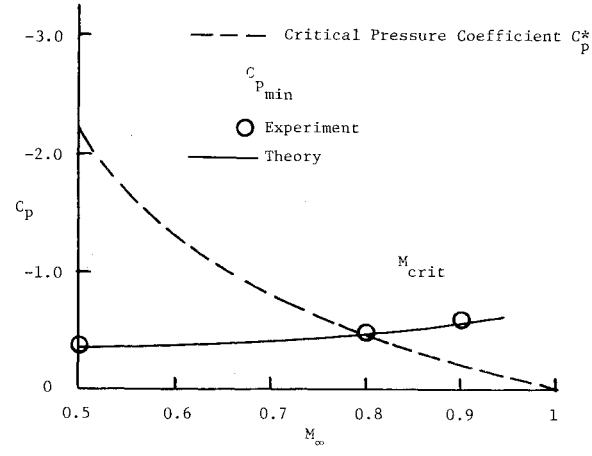

Fig. 10 Predication of critical Mach number for M117 store.

for the preceding bodies were made at transonic Mach numbers. When assessing transonic results, the reader should bear in mind that all numerical methods smear out shock discontinuities over 3-4 cells,[7,9,32] unless an explicit shock fitting scheme is used.[33]

Theoretical and experimental results for the parabolic body of revolution at a freestream Mach number of 0.99 are shown in Fig. 7. The body is 40 cells long and 1 cell high. Present numerical studies showed that small deviations in assumed wind tunnel wall location had a significant effect on the minimum pressure magnitude and shock location, as noted in Ref. 33. The calculations in Fig. 7 were made with the wall location given in Ref. 34, from which the experimental data were taken. Considering the apparent turbulence and experimental scatter, the agreement with experiment is excellent.

Figure 8 represents results for the M117 store at a freestream Mach number of 0.9. Two regions of embedded supersonic flow are quite evident, and both are predicted by the theory. The strong shock just downstream of the nose shoulder is smeared out excessively, but this behavior is to be expected because of the coarseness of the grid in this region. Overall agreement is excellent. Figure 9 compares results for the hemispherical nosed store at a freestream Mach number of 0.8. Except for the slight overexpansion at the nose shoulder, the agreement with experimental data is excellent. The deviations at the nose shoulder are not significant in light of the fact that only 5 cells were used to model this region of severe flow gradients.

Predictions of Critical Mach Number

Figure 10 presents a plot of predicted minimum pressure coefficient versus freestream Mach number for the M117 store. The theory is compared to experimental points from the data of Ref. 35, and the critical Mach number for the configuration is determined by finding the intersection of the minimum pressure curve with the critical pressure coefficient. The agreement between calculated minimum pressure coefficients and available experimental values are excellent.

The critical pressure coefficient is theoretically

$$C_p^* = \frac{2}{\gamma M_\infty^2}\left\{\left[\left(1+\frac{\gamma-1}{2}M_\infty^2\right)\Big/\left(1+\frac{\gamma-1}{2}\right)\right]^{\gamma/(\gamma-1)} - 1\right\} \quad (30)$$

and from plots similar to Fig. 10, the critical pressure coefficient for a particular shape may be accurately predicted. Note that this procedure, if done experimentally for a family of store configurations, would require excessive wind tunnel time, detailed pressure models, and extensive data reduction.

Computational Parameters

Significant computational parameters for the various cases are given in Table 1. The computation times for the subcritical flows in Figs. 3-6 varied from 3 to 10 min on an IBM 370/158 computer, depending on the body shape and freestream Mach number. These times are for the complete solution of a problem, including geometry and grid generation. Computation time for a specific Mach number is significantly reduced when a series of calculations are being made to determine M_{crit}. This is a result of two factors: 1) the

Table 1 Computational Parameters

Configuration	M_∞	Body cells	Total cells X	Total cells Y	Coordinate stretching	Initial conditions	Execution time
Parabolic body[b]	0.8	40	140	18	y only	ρ_∞ V_∞	2 min 44 s
	0.99	40	140	18	y only	ρ_∞ V_∞	5 min 25 s
M117 standard[b] store	0.5	40	140	50	None	ρ_∞ V_∞	4 min 21 s
	0.8	40	140	50	y only	ρ_∞ V_∞	4 min 45 s
	0.9	53	140	50	None	ρ_∞ V_∞	12 min 11 s
16 in. maximum vol.[b] bomb	0.5	68	140	50	None	S.B.T.	9 min 54 s
	0.8	68	140	50	None	S.B.T.	13 min 58 s
Murman-Cole[7] 6% circular arc[c]	0.817	40	74	41	x and y	Previous calculations	30 min
South-Jameson[19] body similar to M117[d]	0.83	Unknown	193	49	Special coordinates	Unknown	3 min 30 s[a]

[a] An average time with mesh halving. [b] IBM 370/158. [c] IBM 360/44. [d] CDC 6600.

geometry, grid generation, and initial condition calculations are only performed once, and 2) for successive Mach numbers, the previously converged solution is used for the initial flowfield. The computation times generally increased as the freestream Mach number was increased, and doubled when embedded shocks were present. The longest subcritical computation time was for the maximum volume hemispherical nosed store; this was attributed to the large velocity gradients in the nose region. In separate computer solutions, the computation times for the M117 store decreased from 10 to 20% when slender body theory was used for initial conditions rather than starting the problem from freestream values.

For all cases investigated, except the parabolic body of revolution, the total grid size was 140×50 cells. The number of cells along the bodies in the flow direction varied from 20 to 68 as dictated by the body fineness ratio. Other computer solutions also showed that coordinate stretching to "infinity" was unnecessary as long as embedded supersonic regions did not extend aft of the body.

Comparisons with Other Methods

Computational parameters for two other finite difference relaxation methods are presented at the bottom of Table 1. Some results from the pioneering work of Murman and Cole[7] are shown for two-dimensional flow over a 6% circular arc airfoil. The computation time is much greater than for any of the present work even though their method had fewer total grid points (or cells) per configuration. The Murman-Cole method used the transonic small disturbance equation rather than the full potential equation, and transonic computations were started using the results of previous subcritical solutions. Their method was also more complex and used nonlinear coordinate stretching in both directions, circle plane mapping, and special treatment of the far-field boundaries.

Results of South and Jameson[19] are also given for a body similar to the M117 store. No specific computation time for this case was given, so an "average" estimate was made based on a given computation time per grid point and total number of iterations. This result includes successive mesh halving, although the authors state that, without mesh halving, the computation times increase by at least a factor of five with noticeable decrease in accuracy. The method employed three different coordinate systems on the various sections of the body, and was designed specifically for blunt body transonic solutions of the full potential equation.

Conclusions

The objective of the current work was to develop an accurate, computationally efficient method for solving the full nonlinear potential flowfield over general bodies at near-critical Mach numbers. The capability, speed, and accuracy of the computational procedure presented in this work are demonstrated by numerical examples which are compared to experiment. The finite volume formulation of the governing equation and the resulting computational procedure eliminate many of the classical problems associated with numerical analysis of fluid flows. The results include three-dimensional axisymmetric flows at subsonic and low transonic speeds, over both pointed and blunt nosed configurations. All numerical results compare well with experiment, particularly for subcritical freestreams. The correlation between theory and experiment is remarkably good considering the possibilities for wind tunnel interference, viscous effects, and the inevitable inaccuracies in model construction and data acquisition. Although not specifically designed for transonic flows, shock strengths and locations are adequately predicted by the theory and do not produce any significant "overshoot" error. Proper consideration of the domain of dependence for density interpolation allows the use of central differences for the velocity, even at locally supersonic points. Computational times are shorter than those for other methods when all factors such as relative computer speeds, number of grid points, and special convergence techniques are taken into consideration. The computer program is simple and involves no complicated numerical schemes or empirical techniques. No problems were encountered for blunt body boundary conditions for grid points near the radial axis, and no special treatment, as is generally required for these regions[19,36] was necessary.

Critical Mach numbers and critical pressure coefficients are predicted easily and accurately, even for blunt hemispherical nosed bodies. This capability may eliminate many costly experimental tests for certain shaped stores. Successive Mach number runs require very little computation time since the grid system is generated only once and calculations for the next Mach number are begun with the previous converged solution.

References

[1] Martin, F.W., Saunders, G.H., and Smith, C.J., "Image System Solution for Store Aerodynamics with Interference—Part I," *Journal of Aircraft*, Vol. 12, March 1975, pp. 151-155.

[2] Martin, F.W. and Walkley, K.B., "Image System Solution for Store Aerodynamics with Interference—Part II," *Journal of Aircraft*, Vol. 12, March 1975, pp. 156-161.

[3] Moore, F.G., "Aerodynamics of Guided and Unguided Weapons, Part I—Theory and Application," NWL TR-3018, Dec. 1973.

[4] Liepmann, H.W. and Roshko, A., *Elements of Gasdynamics*, John Wiley & Sons, Inc., New York, 1957.

[5] Spreiter, J.R., and Alksne, A.Y., "Thin Airfoil Theory Based on Approximate Solution of the Transonic Flow Equation," NACA Rept. 1359, 1958.

[6] Spreiter, J.R., and Alksne, A.Y., "Slender Body Theory Based on Approximate Solution of the Transonic Flow Equation," NASA TR-R-2, 1959.
[7] Murman, E.M., and Cole, J.D., "Calculation of Plane Steady Transonic Flows," *AIAA Journal*, Vol. 9, Jan. 1971, pp. 114-121.
[8] Magnus, R., and Yoshihara, H., "Inviscid Transonic Flow Over Airfoils," *AIAA Journal*, Vol. 8, Dec. 1970, pp. 2157-2161.
[9] Feldman, L.A., and Burkhalter, J.E., "Numerical Solutions of Transient Aerodynamic and MHD Phenomena," AIAA Paper 78-1176, 1978.
[10] Heubner, K.H., *The Finite Element Method for Engineers*, John Wiley & Sons, Inc., New York, 1975.
[11] Shen, S.F., "An Aerodynamicist Looks at the Finite Element Method," *International Symposium on Finite Element Methods in Flow Problems*, University of Alabama Press, 1974.
[12] Leonard, J.W., "Finite Element Analysis of Perturbed Compressible Flow," *International Journal of Numerical Methods in Engineering*, Vol. 4, No. 1, 1972.
[13] Tai, T.C., "Transonic Inviscid Flow over Lifting Airfoils by the Method of Integral Relations," *AIAA Journal*, Vol. 12, June 1974, pp. 798-804.
[14] Crown, J.C., "Calculation of Transonic Flow over Thick Airfoils by Integral Methods," *AIAA Journal*, Vol. 6, March 1968, pp. 413-423.
[15] Neuberger, J.W., "Projection Methods for Linear and Nonlinear Systems of Partial Differential Equations," *Lecture Notes*, Springer-Verlag, to be published.
[16] Neuberger, J.W., "Nonlinear Systems and Projections into Finite Dimensional Sobolev Spaces," 1977, to be published.
[17] Neuberger, J.W., "Partial Differential Equations and Projections of Nonconservative Vector Fields onto Conservative Vector Fields," 1977, to be published.
[18] Neuberger, J.W., "Potential Theory on Finite Grids and Iteration for Nonlinear Systems," 1977, to be published.
[19] South, J.C., and Jameson, A., "Relaxation Solutions for Inviscid Axisymmetric Transonic Flow over Blunt or Pointed Bodies," *Proceedings of the AIAA Computational Fluid Dynamics Conference*, 1973, pp. 8-17.
[20] Ballhaus, W.F., Jameson, A., and Albert, J., "Implicit Approximate-Factorization Schemes for Steady Transonic Flow Problems," *AIAA Journal*, Vol. 16, June 1978, pp. 573-579.
[21] Rizzi, A., "Transonic Solutions of the Euler Equations by the Finite Volume Method," *Symposium Transsonicum II*, Springer-Verlag, Berlin, 1976.
[22] MacCormack, R.W., "Numerical Solution of the Interaction of a Shock Wave with a Laminar Boundary Layer," *Lecture Notes in Physics*, Vol. 8, Springer-Verlag, Berlin, 1971.
[23] Jameson, A., and Caughey, D.A., "Finite Volume Method for Transonic Potential Flow Calculations," AIAA Paper 77-635, June 1977.
[24] Martin, E.D., "Advances in the Application of Fast Semidirect Computational Methods in Transonic Flows," *Symposium Transsonicum II*, Springer-Verlag, Berlin, 1976.
[25] Jameson, A., "Numerical Calculation of the Three Dimensional Transonic Flow Over a Yawed Wing," *Proceedings: AIAA Computational Fluid Dynamics Conference*, 1973, pp. 18-26.
[26] Chen, A.W., Dickson, L.J., and Rubbert, P.E., "A Far Field Matching Method for Transonic Computations," AIAA Paper 77-208, 1977.
[27] Langley Research Center, "Aerodynamic Analyses Requiring Advanced Computers," NASA SP-347, 1975.
[28] Prozan, R.J., Spradley, L.W., Anderson, P.G., and Pearson, M.L., "The General Interpolants Method: A Procedure for Generating Numerical Analogs of the Conservation Equations," AIAA Paper 77-642, 1972.
[29] Conte, S., and de Boor, C., *Elementary Numerical Analysis*, McGraw-Hill, New York, 1965.
[30] Roache, P.J., *Computational Fluid Dynamics*, Hermosa Publishers, Albuquerque, N.M., 1972.
[31] Ashley, H. and Landahl, M., *Aerodynamics of Wings and Bodies*, Addison-Wesley, Reading, Mass., 1965.
[32] Murman, E.M., "Analysis of Embedded Shock Waves Calculated by Relaxation Methods," *AIAA Journal*, Vol. 12, May 1974, pp. 626-633.
[33] Elzweig, S., and Baronti, P., "An Investigation of Wall and Back Pressure Effects in Transonic Interference," GASL TR 245, General Applied Science Laboratories, Inc., June 1977.
[34] Taylor, R.A., and McDevitt, J.B., "Pressure Distributions at Transonic Speeds for Parabolic-Arc Bodies Having Fineness Ratios of 10, 12, and 14," NACA TN 4234, 1958.
[35] Mattasits, G.R., "Aerodynamic Interference Effects on Various Weapon Shapes in the Flow Field of a Transonic Wing Configuration at Mach Numbers from 0.5 to 1.3," AFATL-TR-75-88, 1975.
[36] Abbett, M.J., "Boundary Condition Calculation Procedures for Inviscid Supersonic Flow Fields," *Proceedings: AIAA Computational Fluid Dynamics Conference*, 1973, pp. 153-172.

Make Nominations for an AIAA Award

THE following awards will be presented during the AIAA 13th Fluid and Plasmadynamics Conference and the AIAA 15th Thermophysics Conference, respectively, July 14-16, 1980, Snowmass, Colo. If you wish to submit a nomination, please contact Roberta Shapiro, Director, Honors and Awards, AIAA, 1290 Avenue of Americas, N.Y., N.Y. 10019 (212) 581-4300. The deadline date for submission of nominations is December 3.

Fluid and Plasmadynamics Award

"For outstanding contribution to the understanding of the behavior of liquids and gases in motion and of the physical properties and dynamical behavior of matter in the plasma state as related to needs in aeronautics and astronautics."

Thermophysics Award

"For an outstanding recent technical or scientific contribution by an individual in thermophysics, specifically as related to the study and application of the properties and mechanisms involved in thermal energy transfer within and between solids, and between an object and its environment, particularly by radiation, and the study of environmental effects on such properties and mechanisms."